https://doi.org/10.1016/j.applthermaleng.2018.02.020

Highlights

1. A new modified direct shear test table has been created.
2. A new model has been created for analyzing PGHE's thermo-mechanical performance.
3. The thermo-mechanical performance of PGHE should be fully considered in design.

Title: Simulation of thermo-mechanical performance of pile geothermal heat exchanger (PGHE) considering temperature-depend interface behavior

Authors: Deqi Wang [a], Lin Lu [a,] * and Ping Cui[b,c]

[a] Department of Building Services Engineering, The Hong Kong Polytechnic University, Hong Kong, China

[b] Key Laboratory of Renewable Energy Utilization Technologies in Buildings, Ministry of Education, Jinan, China

[c] School of Thermal Energy Engineering, Shandong Jianzhu University, Jinan, China

* Corresponding author

Tel.: +852-3400 3596; Fax: +852-2765 7198.

E-mail address: vivien.lu@polyu.edu.hk.

Keywords: Ground-coupled heat pump, Pile geothermal heat exchanger, Thermo-mechanical performance, Energy pile

Abstract

Pile geothermal heat exchanger (PGHE) has attracted great interests in recent years, but some new challenges have emerged with its application, especially in understanding its thermo-mechanical behaviors. In this paper, based on the experimental data from a modified direct shear test, a finite element simulation model is developed to investigate the thermo-mechanical behavior of PGHE. The simulation model has been verified by an in-suit test. The influence of interface behavior, thermal loads, and soil properties on the PGHE's thermo-mechanical behavior has been investigated. The results show that the changes in contact force and friction coefficient has to be considered in a comprehensive way in estimating the influence of thermal load on the bearing capacity of PGHE. Compared with the results without thermal loads, bearing capacity of PGHE shows a decreasing ratio of 8.7%, and an increasing ratio of heating is found to be 13.2%. In addition, the simulation results suggest that without head load imposed, at a certain depth, the axial stress has a linear relationship with the change of temperature, but when a head load is imposed, the linear relationship is only separately valid in each temperature region (heating or cooling). The thermo-mechanical performance of PGHE should be fully considered during the design stage, and this paper has the certain actual reference significance to engineering applications.

1 Introduction

As the latest and a popular application of domestic heating/cooling technology [1], the ground-coupled heat pump (GCHP) utilizes the shallow ground to act as a heat sink or source, and is mainly composed of three parts: 1) a heat pump, 2) a geothermal heat exchanger (GHE) as well as 3) a terminal distribution system. The GHE is the core component in the whole system which links the heat pump unit with the ground heat sink, distinguishing the GCHP from the traditional heat pump systems using air as the heat source. The most common type of GHE is the borehole GHE, with each borehole's diameter ranging from 100mm to 150mm and its depth from 15m to 180m, and each borehole contains one or two high strength polyethylene tubes [2].

The borehole GHE can be widely applied under necessary conditions, that is, there is enough space in the ground that can be drilled or trenched. However, the borehole is generally more than 100m deep to save occupied space, thus requiring special drilling equipment and experienced contractors, usually with a very high installation cost. In some cases, over 45% of the total budget for constructing the whole GCHP system could be spent on the installation operation alone. And the cost is even higher when the complicated topography is encountered. To achieve better cost-efficiency, engineers have designed a novel type of GHE, called pile geothermal heat exchanger (PGHE), or energy pile, where the pipes for heat exchange are buried in foundation piles, as shown in **Figure 1**.

With the application of PGHE, some new challenges have emerged, especially in modeling its thermal and thermo-mechanical behaviors. The latest substantial researches concerning thermal behaviors of PGHE can be seen in the developments of models using the “solid” cylindrical heat [3], the spiral source model [4] as well as the composite ring-coil source model [5]. But researches on its thermo-mechanical aspects are still under way. Laloui et al. [6] carried out the first test on the combined thermal and thermo-mechanical performance of a PGHE during a building’s construction stage. They found that the axial load was more than doubled with a rise in temperature of about 15℃ during the applied thermal cycle. Another on-site test was conducted by Bourne [7] involving an instrumented PGHE. However, the result of this particular test contradicted that of Laloui, where the movement of the pile was barely constrained at either end, leaving it drifting in the ground. Additionally, a centrifuge lab test suggested that the bearing capacity [8] of the pile was greatly influenced by the shift in temperature, of which no further explanation was given by the author. The thermo-mechanical behavior observed in the above-mentioned on-site experiment can be explained by a simple geotechnical analysis theory proposed by Knellwolf et al. [9] as an extension of the load-transform method [10, 11]. It is worth pointing out that this method can only be applied under the premise that the behavior of the soil-pile interface is assumed to be a known condition and does not change with temperature. So far, researches on the thermo-mechanical behavior have mainly focused on the thermal-induced stress changes within PGHE [12-14], but very few have considered the change of behavior of the pile’s interface, which could be closely related to the pile’s settlement and its bearing capacity.

To fill this gap, this paper specifically developed a modified version of the direct shear apparatus in order to identify the behavior of the concrete-soil interface. Two different types of soils were examined, and the test results were analyzed. Then based on the experiment data, a finite element model is established to investigate the influences of thermal loads, applied mechanical loads and soil properties on the thermo-mechanical behaviors of PGHE, including the thermal induced stress, friction stress, and bearing capacity by simulating different scenarios. Finally, the simulation results are analyzed and discussed in this paper.

Figure 1 A GCHP Schematic with the PGHE.

2 Behaviors of soil-concrete interface in various thermal loading conditions

The behavior of soil-concrete interface is a critical parameter in geotechnical analysis, especially in determining the pile foundation's maximum bearing capacity. This interface is generally a thin zone of soil, with a thickness of usually 5 to 10 folds of the diameter of average particles [15]. And the properties of the boundaries between the zone and the surrounding soil are mainly decided by the conditions of the latter. Different mechanical parameters, such as the soil density, structure roughness, volumetric response and normal stress were investigated [16, 17] in this research, but the extent to which the temperature influenced the interface was not fully understood. In fact, the soil temperature near the PGHE fluctuated greatly during the operation of GCHP system, suggesting that the thermally induced change of the interface behavior should be investigated first experimentally before the numerical simulations of PGHE.

To quantify the shear strength of concrete and soil, the direct shear test is a very effective way, especially with the aid of a modified direct shear apparatus (MDSA). When a temperature controlling function is applied to form a new shear apparatus, it is named as Modified Direct Shear Apparatus with Temperature control (MDSA-T). This study sampled red clay and Quartz sand, two typical soil, and tested the behaviors of the interfaces between them and concrete separately. Specifically, they were first heated and then cooled to reveal the differences.

2.1 The modified direct shear apparatus with temperature control

The MDSA is a suction-controlled direct shear device proposed by Borana [18]. The shear boxes are isolated from the external environment (atmospheric condition) by an airtight chamber so that the axis-translation technology can be applied to control the suction of soil. The shear force and pressure were measured by two load cells in vertical and horizontal directions, while displacements in the horizontal and upright directions were measured and recorded by two linear voltage displacement transformers (LVDT) during the test. Different from the previous apparatus, the new MDSA-T is a temperature control system designed to simulate the process of PGHE, which can be realized using a heating/cooling box placed at the bottom of the shear box and a heat pump with high precision. Two pipes with thermal insulation layers are utilized to link the heating/cooling box with the heat pump enabling the transportation of chilled and hot water into the heating/cooling box during the cooling and heating simulation.

Temperature response in the air chamber was measured using several thermocouples installed throughout the process of the shearing test, as shown in **Figure 2**. One thermocouple was installed between two boxes piled together vertically, and the other was fixed inside the air chamber so that it could record the real-time interior temperature. The calibration of all the sensors had been conducted before the interface test.

To ensure that the humidity within the air chamber remained unchanged during the test, a solution circulation system was applied. Through installing an air circulation pump with a flow rate of up to 1 L/min in the chamber, the effect of mass-heat transfer was improved. To acquire a detailed record of the transfer, more sensors were installed within the box to track the humidity and temperature levels. All measured data were recorded by a data logger during the whole experiment. The schematic diagram is shown in **Figure 3**.

Figure 2 Schematic diagram of (a) new DSA-T and (b) temperature monitoring sensors.

Figure 3 Mechanism of test-running and data-collecting for the MDSA-T**.**

The design of the air chamber aimed to provide enough space for the boxes used to monitor heating/cooling conditions, shear aspects, and air/solution. **Figure 3**(a) shows the arrangement of the upper box and lower box plate in the shear box, two components commonly seen in the traditional direct shear apparatus. The former is fixed to the horizontal load cell, while the latter is placed on sideways, together with the solution box and heating/cooling box. These two parts were separated during the shear test, with a square section of 100×100×30 mm^3 in the upper box designed to accommodate the soil sample, and a section of 100×100×20 mm^3 in the lower box plate set aside for the concrete sample.

2.2 Test materials and program

Two typical soils were selected to conduct the interface test. One was the sandy soil, or the quartz sand, extracted from a quarry in China, with a large particle size distribution ranging between 0.008 and 1.0mm. The other was the silty clay, or the red clay, a widely used backfill material in the eastern region of China, which consists of Al_2O_3 (30.03%), Fe_2O_3 (15.2%), MgO (2.09%), K_2O (3.16%), and SiO_2 (46.85%). Samples used in this research were also collected in a clay quarry of China, in Hebei province, to be exact, to ensure the test results of the two soils were comparable. **Table 1** lists all the crucial properties, namely, grain density, liquid limit, maximum dry density, plasticity index, as well as plastic limit, and **Figure 4** illustrates the size distribution curves. The soil samples of both sand and clay were firstly dried in an oven with the temperature set at 105℃ for over 24 hours. Then, the sand was placed in a well-sealed bottle and the dry clay was mixed with distilled water to form the saturated specimens with a target water content of 23%.

Figure 4 The two samples' particle size distribution.

Table 1 Summary of the red clay's crucial properties.

The concrete sample was prepared in the lab in accordance with the JGJ 55-2011 standards [19], with a target density of 2100 kg/m3. Concrete is known as a complex multiphase inhomogeneous material consisting of cement, water, and aggregate. In this test, the mass of the cement and aggregate was designed to be 125g and 250g, respectively, and that of the mixed water was 250g. Considering that the dimension of the sample was quite small, the maximum diameter of aggregate should be less than 1mm, thus the average river sand was selected as the aggregate. Special attention had been paid to the creation of concrete surface. During the test of sand-concrete, the cement-sand mixture was poured on a clear plate of glass to form a smooth surface, which, after the solidification, was first polished by a grinding machine, then cut and mounted into the shear box. In comparison, when testing the clay-concrete, the target surface roughness was designed to be 0.25. To obtain this goal, a sand layer with the target surface was prepared at first by covering a glass plate applied with glue with the sand particles (with target size distribution). After the solidification of glue, the cement-sand mixture was poured on the glass plate to form the concrete sample. In this way, when the cement became solid and was removed from the glass plate, the sand layer adhered to the plate and created a concrete surface with the same roughness. Finally, the concrete sample was cut and polished to a specific dimension to fit into the shear box.

Tests were conducted respectively on the sand-concrete interface and the clay–concrete interface. In the case of sand-concrete, considering that the permeability coefficient of sandy soil is usually high, all the specimens were sheared under the dry condition. As shown in **Figure 5**, the dry sand was firstly remolded on the concrete surface and compacted with five layers. Then, the sandy specimen gradually consolidated, followed by the application of a target thermal load, helping achieve the thermal equilibrium, which had been assumed to take about 24 hours as the chamber system gradually reached a steady state. Finally, shearing of the specimen was performed in a target normal pressure condition. For the second group, the loading path was quite similar, but with small differences in the equilibrium and shearing process. As has been mentioned in the test preparation, the clay soil was mixed with the target water to form a saturated specimen. Thus, the full saturated vapor condition was created after the specimen compacted using a small air circulate pump connected to the solution box. Three thermal loads were considered in this study when testing both the sand-concrete and clay-concrete interfaces, including 8℃, 24℃ and 60℃.

Figure 5 Loading paths of soil-concrete interface tests under different thermal conditions.

The shearing velocity of the interface test, when referring to the ASTM Standard [20], did not have a major influence on the interface behavior test between sand and concrete, because most tests were conducted under drained conditions. Thus the shearing velocity of sand-concrete was set at 0.25mm/min. When it comes to the test of the clay-concrete interface, previous studies suggested [18, 21] that the shearing velocity should be less than 0.01mm/min. Thus, the shear rate in this study was set at 0.006mm/min.

2.3 The frictional properties during tests on the interface behaviors

Figure 6 provides an overview of all the sand-concrete test's results. Obviously, different thermal load conditions were linearly related, and the three experiment lines were approximately the same. Therefore, it can be concluded that the temperature changes did not have an observable influence on the interface behavior between sand and concrete. These results also confirmed that the sand-concrete interface's average friction angle is 25.51° .

Figure 6 Impacts of thermal loads in the sand-concrete interface test on the net normal stress in relation to shear strength.

Figure 7 summarized the results of the test on the clay-concrete interface. Similar to the test of the first group, the shear tests were conducted under respectively the normal, and the heating/cooling conditions. Under each condition, the rise in shear strength was proportional to of the raised amount of normal pressure. However, different from the results of the sand-concrete, the temperature changes induced by the thermal loads greatly influenced both c (the adhesion strength) and δ (the interface friction angle).

Figure 7 Impacts of thermal loads in the clay-concrete interface test on the net normal stress in relation to shear strength.

The experiment data are applied in the following numerical model. It is assumed that the friction angle has a linear relationship with the change of surface temperature. Thus, the friction coefficient (μ_k) can be expressed as:

$$\mu_k = \mu_0 + (T - T_0) \cdot C_\mu \tag{1}$$

where μ_0 is the friction coefficient of room temperature, 0.3183, T_0 is the room temperature, 24℃, and C_μ is assumed to be 0.0026613.

3 Numerical simulation model of PGHE

3.1 Descriptions of the numerical model

A model was designed in the research to simulate the PGHE in order to test its thermo-mechanical properties, which created a single PGHE with a diameter of 1.06m and a depth of 25.8m, similar in dimension to a published in-suite pile test [22]. And a spiral-tube with a loop diameter and spiral pitch of 0.4m was meant to be buried in the PGHE. To save the computational resources, a bunch of ring-coils was used to replace the spiral-tube, as shown in **Figure 8**, and the pile could be regarded as a central symmetry body. The established geometric model of soil was large enough to simulate a semi-infinite boundary condition of the ground. A double depth of the pile was set to be the depth of soil domain, and the radius of soil was 10 times that of the pile.

During the simulation, the heat transfer from GHE to the soil, the augmented stress and strain during the transfer process, and the mechanical performance of GHE in either the pile or the soil should all be taken into consideration. However, the heat exchange's circulating flow was not part of the simulation, because the research mainly focused on the thermo-mechanical test on the pile and soil to determine their performance. The heat transfer from the circulating flow was simplified as a heat flux boundary condition. Hence, only the heat conduction process was simulated in this study, the result of which was calculated based on the transfer differential equation:

$$\rho C_p \frac{\partial T}{\partial t} + \nabla\left(k\nabla T\right) = H \tag{2}$$

where T is the temperature (K), and H is the heat generation/extraction rate (W/m^3).

During the operation of PGHE, the pile deformation and the temperature response were one-way couplings, rendering the mechanical equation dependent on the solution of the thermal equation. A coupled analysis on the thermal-displacement was also conducted by the researchers. A backward difference scheme was adopted to control the temperature in reference to ABAQUS [23], and Newton's method played a crucial role in addressing the coupled issue related to the thermal-stress, where its exact implementation was applied to express the issue with a non-symmetric Jacobian matrix:

$$\begin{bmatrix} K_{uu} & K_{u\theta} \\ K_{\theta u} & K_{\theta\theta} \end{bmatrix} \begin{Bmatrix} \Delta u \\ \Delta\theta \end{Bmatrix} = \begin{Bmatrix} R_u \\ R_\theta \end{Bmatrix} \tag{3}$$

where Δu and $\Delta\theta$ respectively stand for the modifications made concerning displacement and temperature's variations, K is the fully coupled Jacobian matrix's submatrices, while R_u and R_θ signify the vectors of the respective mechanical and thermal residues.

The Coulomb friction model was utilized to simulate the pile-soil friction behavior, which assumed that the two contact elements remained stationary unless the equivalent frictional stress (τ_{eq}) surpassed the critical stress ($\tau_f = \mu_k P$, in which μ_k stands for the friction coefficient while P signifies the pressure on contact). In the case of the former being at least equal to the latter, there is a big chance for a slip, the direction of which corresponds with that of the former, $\tau_i / \tau_{eq} = \gamma_i / \gamma_{eq}$.

3.2 Boundary conditions

As mentioned above, a boundary condition for heat flux can be adopted to express the heat transfer between the circulating fluid and the heat exchange tube. The simulation model applied the heat flux directly on the ring-coil surface. Seven cases with different heat flux were simulated to investigate the heat exchange rate's influence on PGHE's performance in the thermo-mechanical aspect.

The thermo-mechanical behavior of PGHE was measured by a two-layer soil model to determine the extent to which it was shaped by the mechanical properties of soil. The first layer had the same depth with the pile, as illustrated in **Figure 8**, and the second layer under the pile bottom had a different modulus from the first one. **Table 2** provides a series of numbers concerning the major properties. It can be seen that, for the soil bottom, the value of the mechanical boundary condition was fixed, and only the vertical displacement was allowed at the axial and the horizontal outer boundaries. For the interface behavior, two conditions were simulated: one was the constant friction coefficient and the other was the assumption of the friction coefficient which had a linear relationship with the temperature, as expressed by Eq. (1). The simulation is best to be conducted over a relatively longer period, for example, 12 days, because it is unlikely to identify the exact impact made by PGHE's thermo-mechanical behavior within a short term.

Figure 8 Information of spiral-tube-PGHE-generated geometry and mesh.

Table 2 Properties of concrete and soil for simulation.

3.3 Comparison and validation

The proposed simulation model is compared with an in-suit experiment for validation purpose. The experiment was undertaken at École Polytechnique Fédérale de Lausanne (EPFL), Switzerland [6], and carried out during the construction of a new campus's building. Thermal tests were investigated after the construction of each floor, which means the pile was subjected to different head loads during the whole test period. The pile is free to move at the top during the first thermal test (without any head load), and is imposed by a maximum load of 1300kN when the building is completed.

The comparison results between the simulation model and the in-suit test are illustrated in **Figure 9**, **Figure 10** and **Figure 11**. It can be seen that the simulation results agree well with the results from the in-suit tests. In the first thermal test, an increase of temperature is about 20℃ after 12 days of operation. Without head load, a small axial load is mobilized by the restraint of the shaft force. The maximum thermal induced compressive force in the pile found at 17.5m depth. **Figure 10** shows the response of thermal induced axial stress with different temperature increase. The test data of two points which are located at the top (2.5m) and the bottom (21.5m) are selected to compare with the simulation results. The simulation data fits well with the experimental results.

Figure 9 (a) Temperature profile of the first thermal test and (b) axial force profiles at end of heating with free head load, compared with the Lausanne's test.

Figure 10 Variation of pile axial stress in response to temperature, compared with the Lausanne's test.

The comparison results of axial stress profiles with a head load of 1300kN are illustrated in **Figure 11**. The inferred thermal load (ITL) is calculated by the difference between the mechanical load (ML) and the total axial load (TL). As shown in the figure, the mechanical load decreases with the depth, and the numerical stress curve agrees well with the experimental one. For the stress curves of total axial load, except for a big difference occurs at the first point, which might be a consequence of the variations in the diameter of the pile [24], the simulation data can model the thermo-mechanical of PGHE well.

Figure 11 Axial force profiles at end of heating with a head load, compared with the Lausanne's test.

4 Results and discussion

In this study, three groups of simulations are conducted and investigated: 1) Influence of the thermal loads, 2) Influence of the interface behavior and 3) Influence of the soil properties (Young Modulus). The basic simulation parameters are summarized in **Table 3**.

Table 3 The summary of boundary condition and material properties in different simulation cases.

4.1 Influence of the thermal loads

In this section, the main focus is paid to the influence of heating/cooling thermal loads on the thermo-mechanical behavior of PGHE, so it assumed that two soil layers have the same physical property, with a modulus of 26MPa. Seven different thermal loads are investigated (H1=270W/m, H2= 240W/m, H3=150W/m, H4=75W/m, C1=-

106W/m, C2=-75W/m and C3=-38W/m). The simulation results of the corresponding temperature changes are shown **Figure 12**(a). After 12 days, the temperature difference at the interface between pile and soil increases to 36℃ in the case of H1, which is exactly the difference observed in the interface behavior test of heating. For the case of C3, a temperature decrease of 14℃ occurs at the end of cooling. The temperature distribution along the pile depth are illustrated in **Figure 12**(b). It can be seen that the temperature curve along the pile depth is nearly uniform, thus the influence induced by the temperature difference along the pile depth can be neglected.

Figure 12 (a) Temperature response at the interface between pile and soil and (b) along the pile depth with different thermal loads.

The axial stress in the pile and the shear stress at the interface are calculated. Under each case of thermal load, two head load conditions are simulated, i.e., the pile without any vertical head force, or the pile with a head load of 5000kN. In the head load cases, the head load is applied after the equilibration of geostatic pressure, and followed by a constant heat flux imposed over 12days.

Without a head restraining force and thermal load (NT), as shown in **Figure 13**, the axial stress increases linearly with the depth. The pile is restrained by the pile-soil interface and the bottom but to free move at the top, thus either in heating or cooling process only a small axial force is mobilized at the top of pile. When the pile is heated, the pile expends from the null point to top and bottom. To restrict this movement, a ‘positive’ shaft friction is mobilized above the null point and a ‘negative’ one occurs below the point (the ‘positive’ means the force direction is from the pile’s top to the bottom). The restraint induced by the interface and bottom generates additional compressive axial load, which increases with the thermal loads. The maximum stress (compressive) of about 1841kPa is developed around the two-thirds depth (17.0m) of the pile in response to the temperature increase of 36℃. On the contrary, if cooled, the pile will contract. In response to the restriction of the pile-soil interface, tensile stress, negative shear stress (above the null point) and positive shear stress (under the null point) are generated. With a temperature decrease of 14℃, the maximum tensile stress of about 261kPa at the depth of 8.8m.

Figure 13 (a) Axial force profiles and (b) pile shaft friction profiles along the pile depth with different thermal loads (without head load).

The variation of the axial stress with the temperature change is summarized in **Figure 14**. Data are collected from four monitoring points, which located at the depths of 2.5m, 7.5m, 15.0m and 22.5m. In all the heating and the cooling cases, the axial stress has an approximately linear relationship with the change of temperature. For the depth of 7.5m, the observed increase rate of axial stress is -31.5kPa/℃. Owing to the restrain of at pile's bottom, the increase rate of axial at the bottom is larger than that at the top.

Figure 14 Variation of axial stress with different thermal loads (without head load).

With an imposed head load of 5000kN, the distributions of combined thermo-mechanical axial stress with different thermal loads are shown in **Figure 15**(a). If there is no thermal load (NT), the axial load will decrease with the depth, because the pile's shift resistance carrying out most of the load force. Unlike the cases of free head load, only compressive stress is observed in all head load cases. A temperature increase of 36℃ results in a combined thermo-mechanical load of 6139kN in which the thermal induced additional axial stress is 1213kN, that is the maximum axial stress observed among all head load cases. The location of this maximum axial stress is not at the lower-part of the pile, and moves up to 7.2m. Additionally, the results also show that the heating process has a stronger effect on changing the axial stress profile than cooling, in which only a small decrease can be observed above the depth of 15m, and a slight increase occurs under this depth. The reason can be found in **Figure 15**(b). The temperature decrease causes a weakening effect on the pile-soil interaction, and the shift resistance cannot fully restrict the movement induced by the temperature change. To balance the thermal contract, an additional head displacement of 1.6cm is developed in case of C1, and more axial stress is transferred to the pile's bottom. But, for the heating case, the temperature increase can enhance the interface behavior between pile and soil, thus more friction force is mobilized to restrict the thermal induced movement which is -0.6cm in the case of H1.

Figure 15 (a) Axial force profiles and (b) pile shaft friction profiles along the pile depth with different thermal loads (with a head load of 5000kN).

The variation data of additional axial stress induced by thermal load are collected (with the same depths as the cases of free head load), as shown in **Figure 16**. The variation profiles are quite different with that of the cases with the free head load. The linear relationship is no longer valid in the whole temperature region, but separately valid as the cut-off of zero. In heating, the variation profiles are similar to the previous cases, except for an obvious difference at the top, that the stress change induced by the thermal load increase from -15.1kPa/℃ to -17.7kPa/℃ due to the high restrain of the head load. However, in cooling, the variation is totally different, but the linear relationship also exists in the left-half plane. The stress change induced by temperature variation with in pile is between -12.5kPa/℃ to +12.5kPa/℃.

Figure 16 Variation of axial stress with different thermal loads (with a head load of 5000kN).

4.2 Influence of the interface behavior

The interface behavior of soil-pile plays an important role in effecting a pile's shaft frictional force, which provides part of support force to building's structure. The interface behavior, affected by heat exchange, can influence the axial stress and frictional stress distribution of PGHE, and then, influence the bearing capacity of the pile. Therefore, in this section, to investigate the influence of interface behavior, two different conditions are considered (constant friction coefficient-C or functional friction coefficient-F), and the results are summarized in **Figure 17** and **Figure 18**.

The load-displacement (LD) curves, illustrated in **Figure 17**, indicate that the bearing capacity of PGHE is overestimated when the friction coefficient is regarded as constant. The displacement of the reference curve (NT) increases greatly after the head load of about 4956kN which could be regarded as the bearing capacity of normal temperature. It can be seen clearly that even when assuming the friction coefficient does not change with temperature, the cooling process has a weaken effect on the bearing capacity of PGHE with a decrease ratio of 4.6% responding to a temperature change of -14℃. A 7.1% increase is found in the heading case with a temperature increase of 36℃. These changes should be the consequence of cold-contraction and heat-expansion of PGHE, and this thermal induced deformation directly influences the contact force at the pile-soil interface. As shown in **Figure 18**, the average decrease ratio of contact force (Cooling-C) is 2.3%. It can also be noted that the change of contact force is independent with the friction coefficient, but only related to temperature change.

When taking the temperature dependent friction coefficient into consideration, the thermal induced influence on the bearing capacity is enhanced. The decreasing ratio is up to 8.7%, which is almost twice than that of the constant case, in cooling case, and the increasing ratio of heating grows to 13.2%. Theses figure clearly show that the influence of temperature on the pile-soil interface behavior should be comprehensively considered. The thermal induced change of bearing capacity is determined by a composite impacts of the contact force and the friction coefficient, not simply influenced by the thermal expansion or contraction of concrete.

Figure 17 Load displacement curves with different interface conditions.

Figure 18 Contact force profiles with different interface conditions.

The related axial stress and the shear stress profiles are presented in **Figure 19**. With a strong shaft force, it is not surprised that the additional axial load induced by thermal load in Heating-F is greater than that in Heating-C. In the case of Cooling-F, pile shows an increase of axial stress in the section under 15m, and a decrease above this depth, indicating that pile moves downwards with the decrease of shaft force, and more axial load transfers from the top to the bottom.

Figure 19 (a) Axial force profiles and (b) pile shaft friction profiles along the pile depth with different interface conditions (with a head load of 5000kN)

4.3 Influence of the soil properties (Young Modulus)

Four groups of cases with different modulus of the surrounding soil (Soil-1) and bottom soil (Soil-2) are simulated. E-0 is the modulus used in the previous simulations cases (section 4.1 and 4.2). The calculated axial force and pile shaft force are illustrated in **Figure 20**. The results show that the modulus of soil can affect the thermo-mechanical performance of PGHE significantly, even with in a small region of values.

Similar to the previous results, the change of modulus has a more notable influence on axial load distribution in the heating phase. It can be seen that, in **Figure 20**(a), compared with the case of H-E0, when the bearing layer has a high stiffness, the layer provides more support at the pile toe. As a consequence, mobilized shaft stress is less and more axial load transfers from the top to the bottom. When modulus of the bearing layer changes from 26Mpa to 260Mpa, the additional axial load (at the toe) induced by temperature change increases from 1009.23kPa (H-E0) to 2878.89kPa (H-E3). But, no big difference is observed in the values of maximum axial stress between these two cases. The results indicate that the modulus of surrounding soil can affect the maximum axial stress more than that of the soil under pile toe. With a high stiffness (H-E1) around pile shaft, more shaft shear stress is mobilized, as shown in **Figure 20**(b). With a high fractional restraint, an additional compressive load is mobilized in the middle of pile. Taking the case of H-E0 as a reference, when the modulus double (H-E1), the additional axial stress increases from 1290kN to 1638kN with an increasing ratio of 27%.

Among the cooling cases, the change of axial stress in the upper part is almost same, and all the profiles show a slight decrease compared with the case without thermal load (NT). Only the stress profile of C-E3 shows an obvious increase at the pile toe, which is similar to the heating case of H-E3. The reason can also be explained that, with a high stiffness at the bottom, more axial load is transferred to the strong bottom layer.

Figure 20 (a) Axial force profiles and (b) pile shaft friction profiles along the pile depth with different soil properties (with a head load of 5000kN).

5 Conclusion

The applications of PGHE have been attracting increasing attentions in recent years, but its thermo-mechanical behavior has not been fully understood. In this paper, based on the experimental data from a modified direct shear apparatus, a finite element simulation model is developed to investigate the thermo-mechanical behavior. The simulation model has been verified by an in-suit test. The influence of the temperature-dependent interface behavior on the pile’s thermo-mechanical behavior has been investigated. In addition, the investigations considering the influence of thermal loads and soil properties are conducted. The main conclusions are summarized as follows:

1) Without imposed head load, at a certain depth, the axial stress has an approximately linear relationship with the change of temperature. For the depth of 7.5m, the observed increase rate of axial stress is -31.5kPa/℃. With an imposed head load of 5000kN, the linear relationship is no longer valid in the whole temperature region, but separately valid as the cut-off of zero.

2) The influence of temperature on the pile-soil interface behavior should be comprehensively considered. The thermal induced change of bearing capacity is determined by a composite impacts of the contact force and the friction coefficient, not simply influenced by the thermal expansion or contraction of concrete. For the condition assumed in this paper, the decreasing ratio of bearing capacity in cooling is up to 8.7% (temperature-depend friction coefficient), which is almost twice than that of case with constant friction coefficient, and the increasing ratio of heating is 13.2%.

3) The results indicate that the modulus of surrounding soil can affect the maximum axial stress more than that of the soil under pile toe. Taking the case of H-E0 as reference, when the modulus double (H-E1), the additional axial stress increases from 1290kN to 1638kN with an increase ratio of 27%. Generally, the thermal induced increase of axial stress is not big enough to pose a threat to the pile’s structure, but more attention should be paid if the soil has a large modulus and a strong interface behavior with pile.

The thermally induced change in bearing capacity should be fully considered for the design of a PGHE system. Special attention should be paid on the cooling operation, a safety factor should be taken into account in the design stage of the PGHE. In this study, the safety factor could be 1.10 to avoid excessive settlement occurring in the cooling operation. However, the results may vary with the types of soil, thus more soil samples will be investigated in the future works. In addition, some stress-concentrated areas have been observed near the ring-coil surface. Under such a great stress, the pile may suffer from the concrete fatigue for the long-term heating/cooling operation. Therefore, the long-term fatigue test should be an important research direction of PGHE system in the future.

Acknowledgments

This work was financially funded by the Hong Kong Research Grant Council through General Research Fund (PolyU 5176/13E).

References

[1] G.-H. Go, S.-R. Lee, S. Yoon, H.-b. Kang, Design of spiral coil PHC energy pile considering effective borehole thermal resistance and groundwater advection effects, Applied Energy, 125 (2014) 165-178.

[2] G. Florides, S. Kalogirou, Ground heat exchangers—A review of systems, models and applications, Renewable Energy, 32 (2007) 2461-2478.

[3] Y. Man, H. Yang, N. Diao, J. Liu, Z. Fang, A new model and analytical solutions for borehole and pile ground heat exchangers, International Journal of Heat and Mass Transfer, 53 (2010) 2593-2601.

[4] Y. Man, H.X. Yang, N.R. Diao, P. Cui, L. Lu, Z.H. Fang, Development of spiral heat source model for novel pile ground heat exchangers, Hvac&R Research, 17 (2011) 1075-1088.

[5] D.Q. Wang, L. Lu, P. Cui, A novel composite-medium solution for pile geothermal heat exchangers with spiral coils, International Journal of Heat and Mass Transfer, 93 (2016) 760-769.

[6] L. Laloui, M. Nuth, L. Vulliet, Experimental and numerical investigations of the behaviour of a heat exchanger pile, International Journal for Numerical and Analytical Methods in Geomechanics, 30 (2006) 763-781.

[7] P.J. Bourne-Webb, B. Amatya, K. Soga, T. Amis, C. Davidson, P. Payne, Energy pile test at Lambeth College, London: geotechnical and thermodynamic aspects of pile response to heat cycles, Géotechnique, 59 (2009) 237-248.

[8] J.E. Rosenberg, Centrifuge modeling of soil-structure interaction in thermo-active foundations, in, University of Colorado at Boulder, 2010.

[9] C. Knellwolf, H. Peron, L. Laloui, Geotechnical analysis of heat exchanger piles, Journal of Geotechnical and Geoenvironmental Engineering, 137 (2011) 890-902.

[10] H.B. Seed, L.C. Reese, The Action of Clay Along Friction Piles, J Geoteh Engng, 504 (1957) 92.

[11] H.M. Coyle, L.C. Reese, Load transfer for axially loaded piles in clayJ of SMFE Div, in: ASCE, Vol. 97, 1966, pp. 1-25.

[12] N. Batini, A.F.R. Loria, P. Conti, D. Testi, W. Grassi, L. Laloui, Energy and geotechnical behaviour of energy piles for different design solutions, Applied Thermal Engineering, 86 (2015) 199-213.

[13] S. Jeong, H. Lim, J.K. Lee, J. Kim, Thermally induced mechanical response of energy piles in axially loaded pile groups, Applied Thermal Engineering, 71 (2014) 608-615.

[14] D. Qi, L. Pu, F. Sun, Y. Li, Numerical investigation on thermal performance of ground heat exchangers using phase change materials as grout for ground source heat pump system, Applied Thermal Engineering, 106 (2016) 1023-1032.

[15] M. Boulon, P. Foray, Physical and numerical simulation of lateral shaft friction along offshore piles in sand, in: Proc. 3rd International Conference on Numerical methods in offshore piling, Nantes, France, 1986, pp. 127-147.

[16] L. Borana, J.-H. Yin, D. Singh, S. Shukla, A Modified Suction Controlled Direct Shear Device for Testing Unsaturated Soil and Steel Plate Interface, Marine Georesources & Geotechnology, (2013).

[17] M.A. Hossain, J.-H. Yin, Behavior of a compacted completely decomposed granite soil from suction controlled direct shear tests, Journal of Geotechnical and Geoenvironmental Engineering, 136 (2009) 189-198.

[18] L. Borana, Study on The Interface Behavior between Unsaturated Soil and Steel Surface, in: Building Service Engineering Vol. PhD, The Hong Kong Polytechnic University, 2013.

[19] W. Ding, F. Leng, Specification for mix proportion design of ordinary concrete (JGJ55-2011), in, China Building Industry Press: Beijing, China, 2011.

[20] A. Standard, D3080/D3080M-11 Standard test method for direct shear test of soils under consolidated drained conditions, West Conshohocken, PA: ASTM International, (2012).

[21] A. Di Donna, A. Ferrari, L. Laloui, Experimental investigations of the soil-concrete interface: physical mechanisms, cyclic mobilisation and behaviour at different temperatures, Canadian Geotechnical Journal, (2015).

[22] L. Laloui, Thermo-mechanical behaviour of soils, Revue Française de Génie Civil,

5 (2001) 809-843.

[23] X. Xu, W. Zhang, Y. Hu, Y. Wang, L. Lu, S. Wang, Preparation and overall energy performance assessment of wide waveband two-component transparent NIR shielding coatings, Solar Energy Materials and Solar Cells, 168 (2017) 119-129.

[24] B.L. Amatya, K. Soga, P.J. Bourne-Webb, T. Amis, L. Laloui, Thermo-mechanical behaviour of energy piles, Géotechnique, 62 (2012) 503-519.

Figures

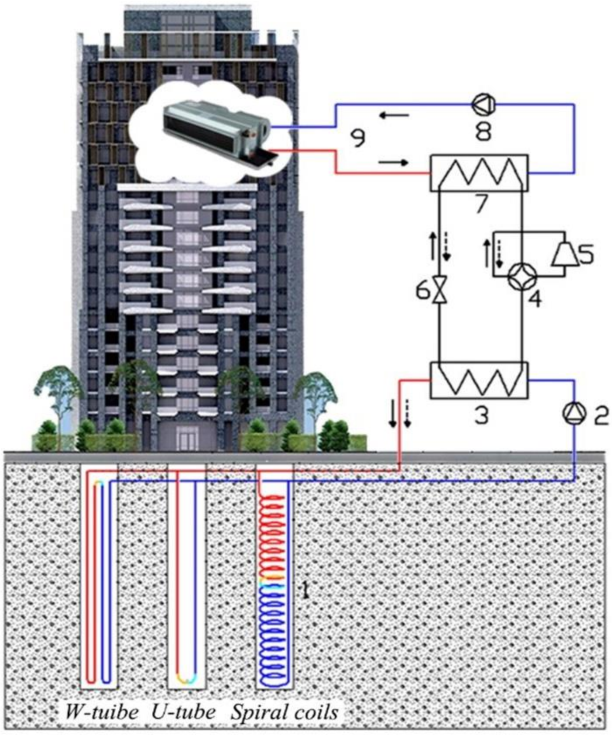

1. PGHE; 2, 8 circulation pump; 3, 7 condenser and evaporator; 4 reversing valve; 5 compressor; 6 expansion valve; 9 terminal device

Figure 1 A GCHP Schematic with the PGHE.

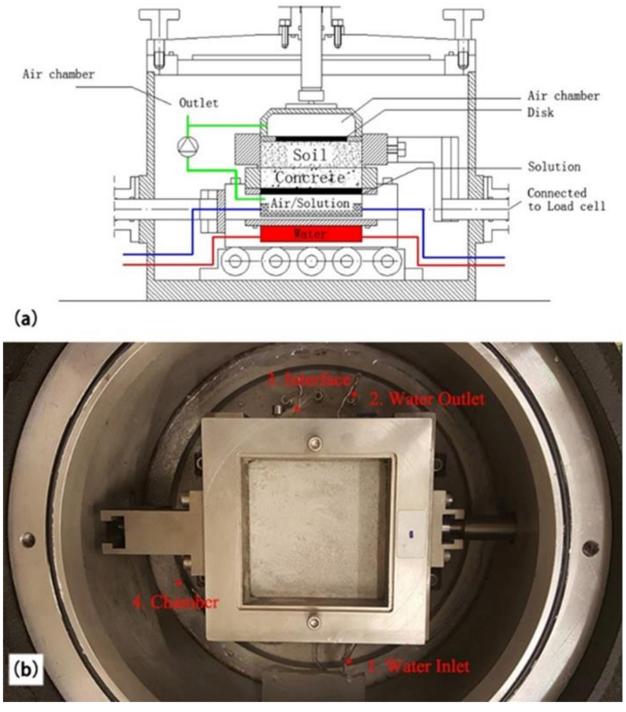

Figure 2 Schematic diagram of (a) new DSA-T and (b) temperature monitoring sensors.

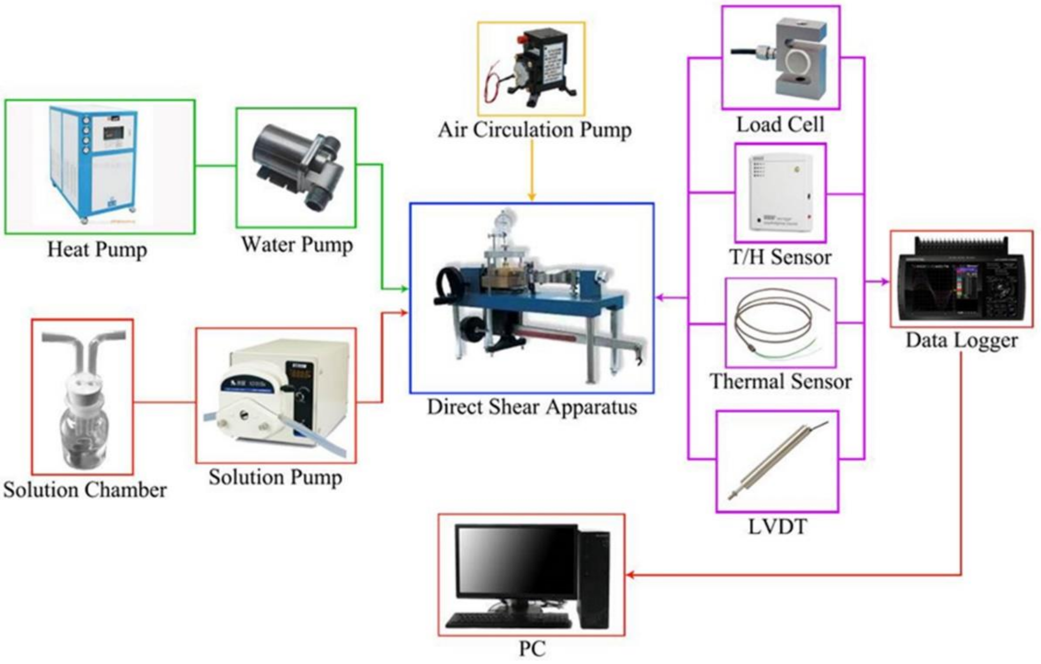

Figure 3 Mechanism of test-running and data-collecting for the MDSA-T**.**

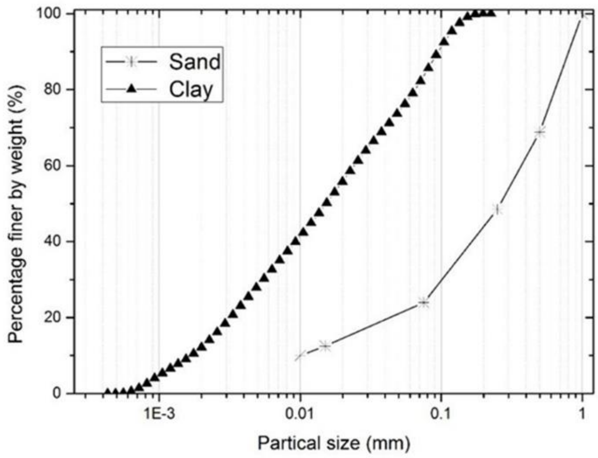

Figure 4 The two samples' particle size distribution.

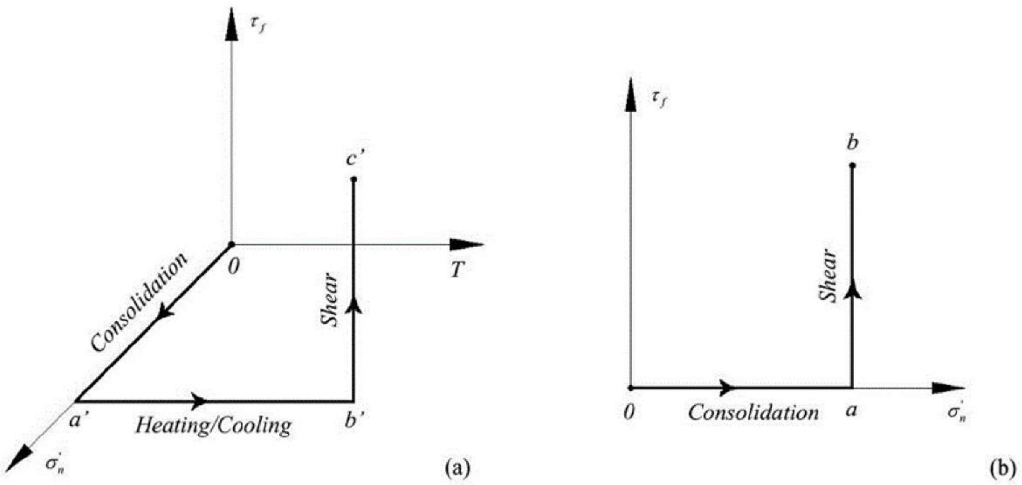

Figure 5 Loading paths of soil-concrete interface tests under different thermal conditions.

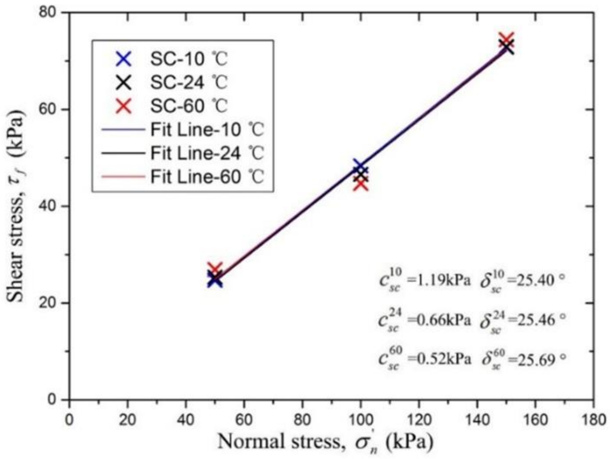

Figure 6 Impacts of thermal loads in the sand-concrete interface test on the net normal stress in relation to shear strength.

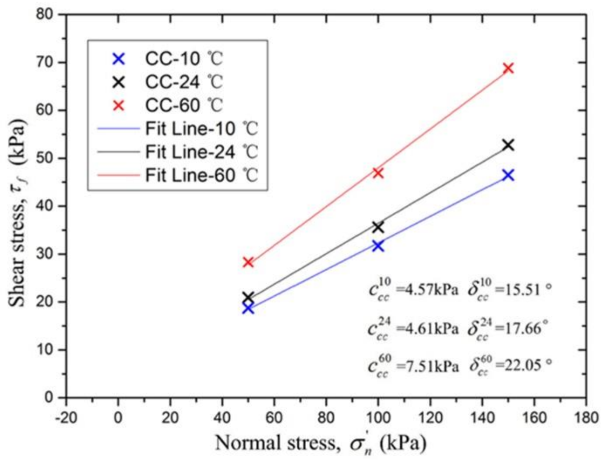

Figure 7 Impacts of thermal loads in the clay-concrete interface test on the net normal stress in relation to shear strength.

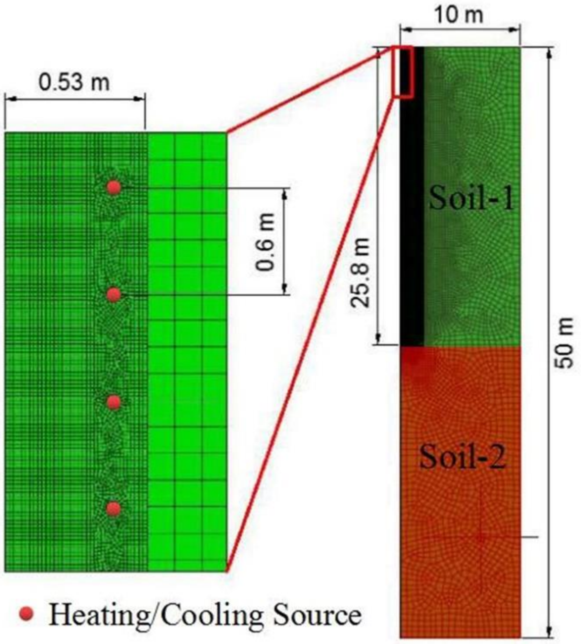

Figure 8 Information of spiral-tube-PGHE-generated geometry and mesh.

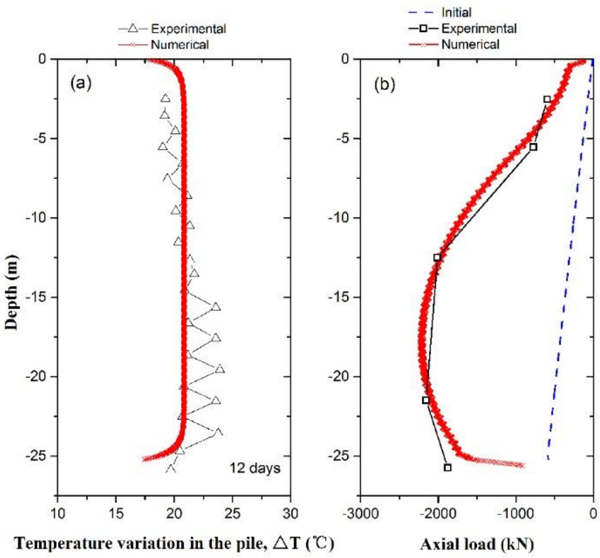

Figure 9 (a) Temperature profile of the first thermal test and (b) axial force profiles at end of heating with free head load, compared with the Lausanne’s test.

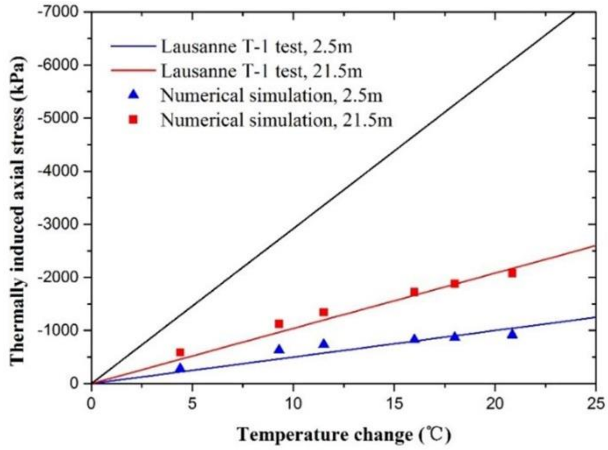

Figure 10 Variation of pile axial stress in response to temperature, compared with the Lausanne's test

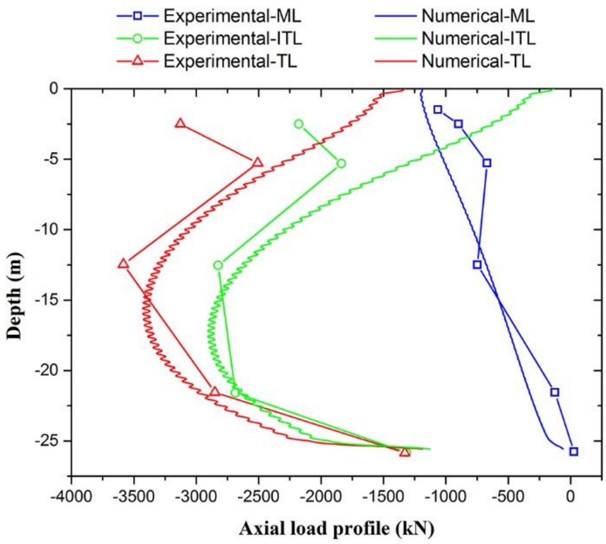

Figure 11 Axial force profiles at end of heating with a head load, compared with the Lausanne's test.

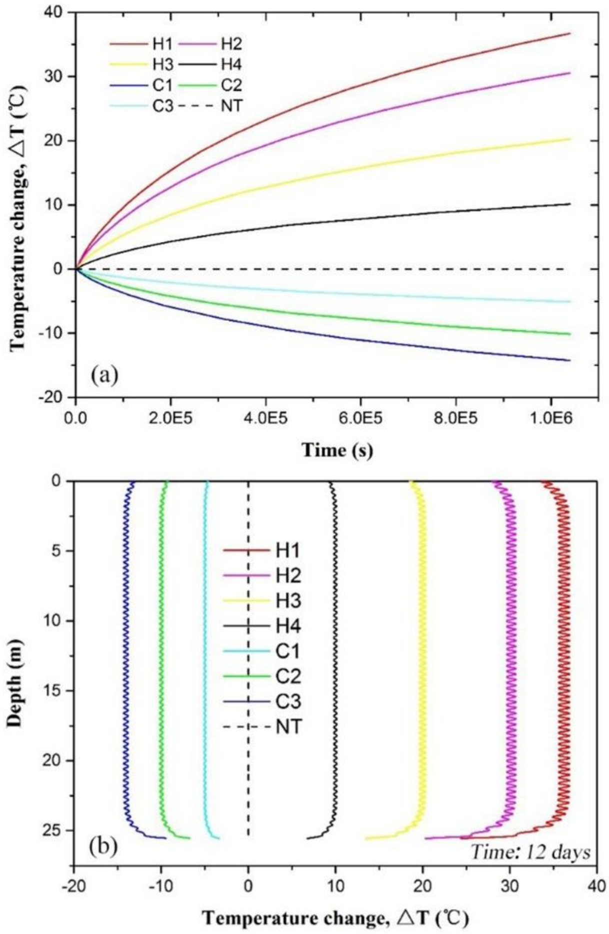

Figure 12 (a) Temperature response at the interface between pile and soil and (b) along the pile depth with different thermal loads.

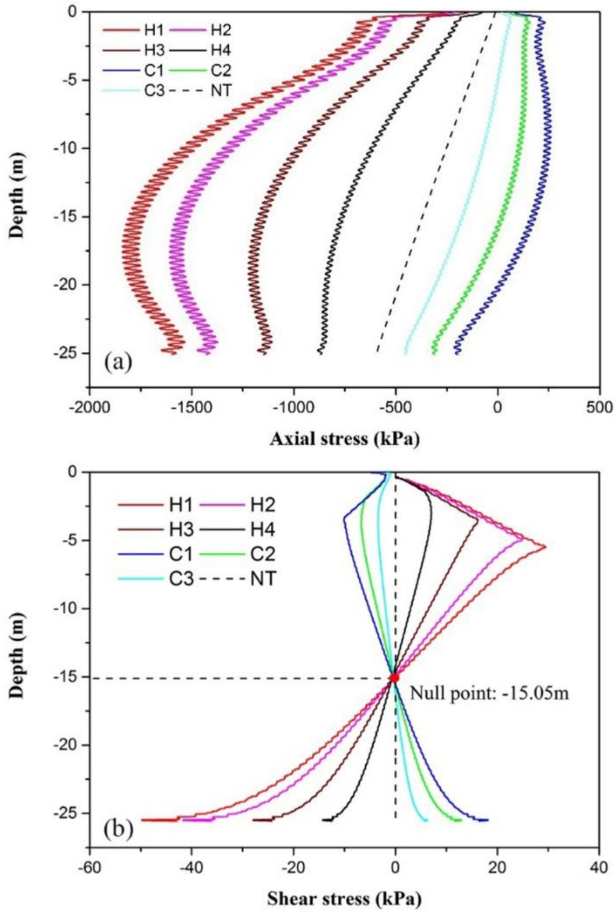

Figure 13 (a) Axial force profiles and (b) pile shaft friction profiles along the pile depth with different thermal loads (without head load).

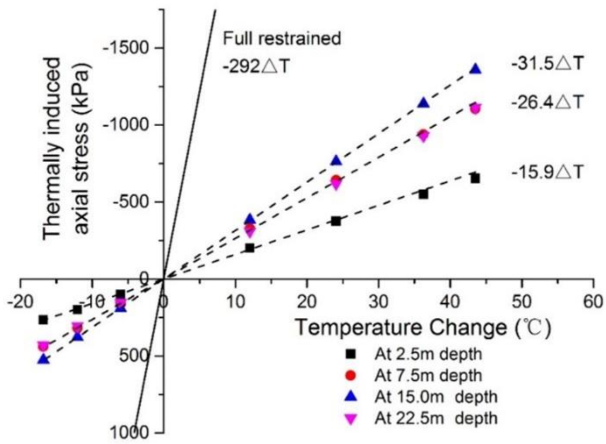

Figure 14 Variation of axial stress with different thermal loads (without head load).

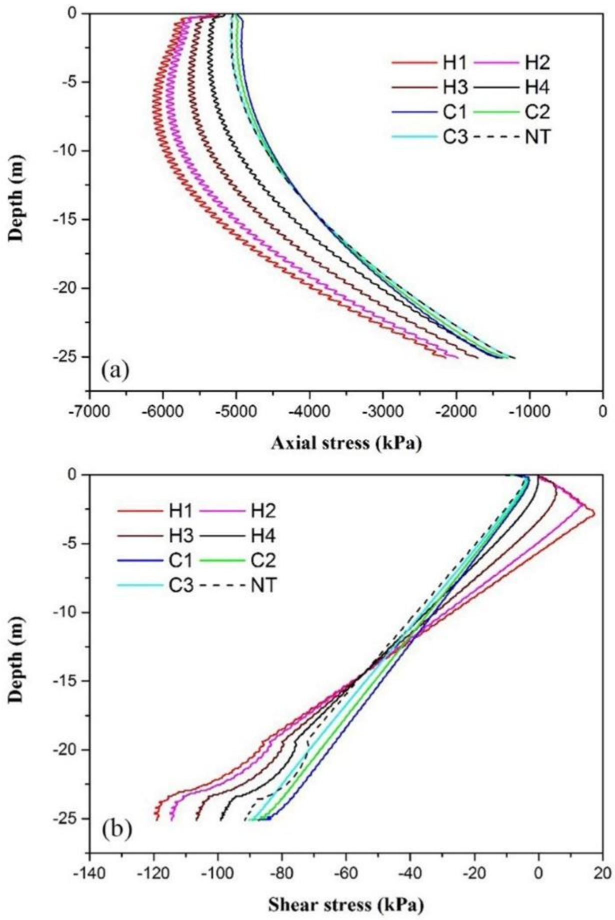

Figure 15 (a) Axial force profiles and (b) pile shaft friction profiles along the pile depth with different thermal loads (with a head load of 5000kN).

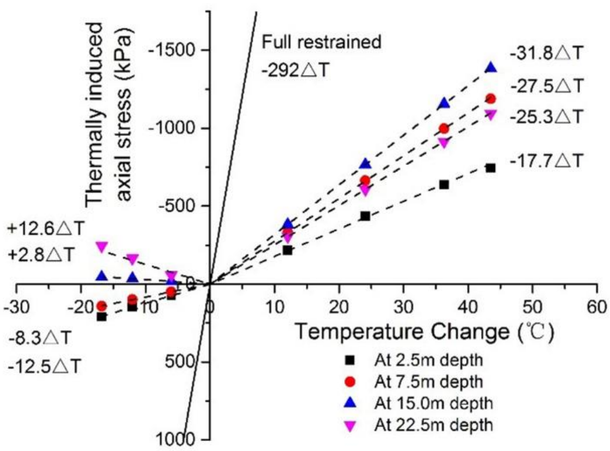

Figure 16 Variation of axial stress with different thermal loads (with a head load of 5000kN).

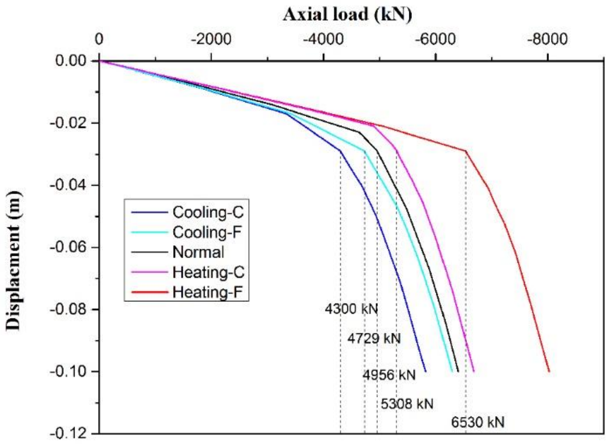

Figure 17 Load displacement curves with different interface conditions.

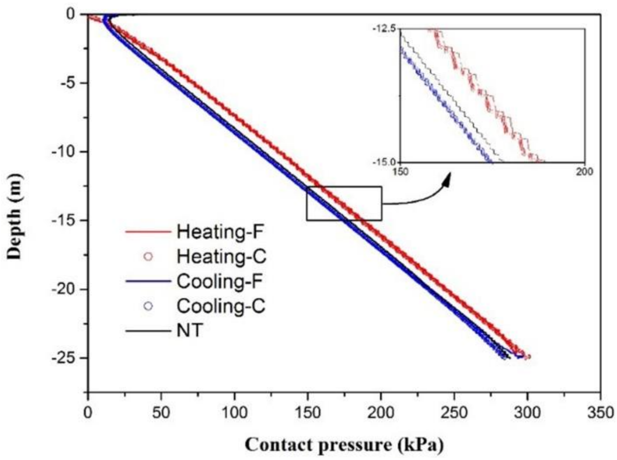

Figure 18 Contact force profiles with different interface conditions.

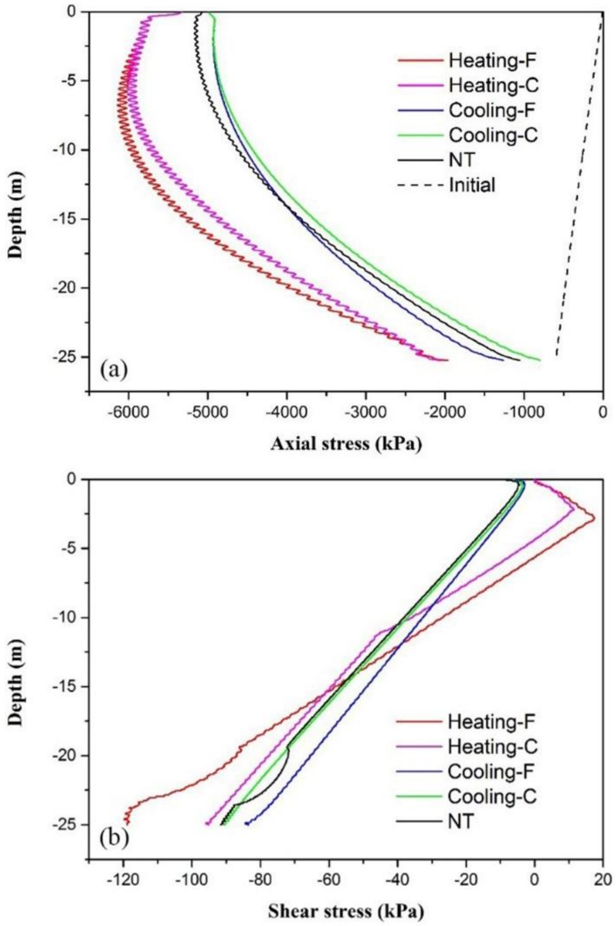

Figure 19 (a) Axial force profiles and (b) pile shaft friction profiles along the pile depth with different interface conditions (with a head load of 5000kN)

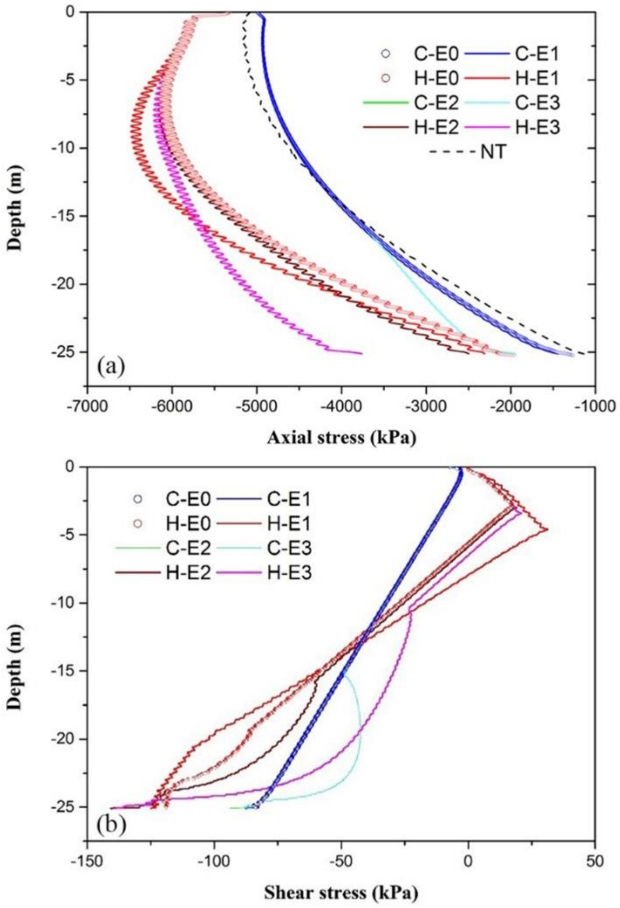

Figure 20 (a) Axial force profiles and (b) pile shaft friction profiles along the pile depth with different soil properties (with a head load of 5000kN).

Tables

Table 1 Summary of the red clay's crucial properties.

Liquid limit	WL [%]	49.5
Plastic limit	WP [%]	22.6
Plasticity index	IP [%]	26.9
95% Clay diameter	D95 [mm]	0.12
Max. dry density	ρm [g]	2.54

Table 2 Properties of concrete and soil for simulation.

Material		Concrete	Soil-1&2
Item	Unit		
Conductivity/*k*	W/(m*K)	1.628	1.82
Density/ *ρ*	kg/m3	2500	2500
Specific Heat/ *Cp*	J/(kg*K)	837	880
Young Modulus/*E*	Pa	2.8E+10	2.6E+07
Poisson's Ratio/*v*	1	0.25	0.35
Friction Angle of Soil/*φ*	°	-	30.5
Cohension of Soil/*c*	kPa	-	20

Table 3 The summary of boundary condition and material properties in different simulation cases.

<table>
<tr><th colspan="2" rowspan="2">Item No.</th><th rowspan="2">Heat flux (W/m)</th><th colspan="3">Young Modulus, E (Pa)</th><th rowspan="2">Friction coefficient</th></tr>
<tr><th>Concrete</th><th>Soil-1</th><th>Soil-2</th></tr>
<tr><td></td><td>NT</td><td>-</td><td>2.92E+10</td><td colspan="2">2.60E+07</td><td>-</td></tr>
<tr><td rowspan="7">Influence of the thermal loads</td><td>H1</td><td>270</td><td rowspan="7">2.92E+10</td><td colspan="2" rowspan="7">2.60E+07</td><td rowspan="7">Function</td></tr>
<tr><td>H2</td><td>240</td></tr>
<tr><td>H3</td><td>150</td></tr>
<tr><td>H4</td><td>75</td></tr>
<tr><td>C1</td><td>-106</td></tr>
<tr><td>C2</td><td>-75</td></tr>
<tr><td>C3</td><td>-38</td></tr>
<tr><td rowspan="4">Influence of the interface behavior</td><td>Heating-F</td><td rowspan="2">270</td><td rowspan="4">2.92E+10</td><td colspan="2" rowspan="4">2.60E+07</td><td>Function</td></tr>
<tr><td>Heating-C</td><td>Constant</td></tr>
<tr><td>Cooling-F</td><td rowspan="2">-38</td><td>Function</td></tr>
<tr><td>Cooling-C</td><td>Constant</td></tr>
<tr><td rowspan="8">Influence of the soil properties</td><td>C-E0</td><td>-38</td><td rowspan="8">2.92E+10</td><td rowspan="2">2.60E+07</td><td rowspan="2">2.60E+07</td><td rowspan="8">Function</td></tr>
<tr><td>H-E0</td><td>270</td></tr>
<tr><td>C-E1</td><td>-38</td><td rowspan="2">5.20E+07</td><td rowspan="2">5.20E+07</td></tr>
<tr><td>H-E1</td><td>270</td></tr>
<tr><td>C-E2</td><td>-38</td><td rowspan="2">2.60E+07</td><td rowspan="2">5.20E+07</td></tr>
<tr><td>H-E2</td><td>270</td></tr>
<tr><td>C-E3</td><td>-38</td><td rowspan="2">2.60E+07</td><td rowspan="2">2.60E+08</td></tr>
<tr><td>H-E3</td><td>270</td></tr>
</table>